*Earthquake Geotechnical Engineering for Protection and Development of Environment and Constructions – Silvestri & Moraci (Eds)*
*© 2019 Associazione Geotecnica Italiana, Rome, Italy, ISBN 978-0-367-14328-2*

# Quantification of the field of shear strains in saturated sand subjected to undrained monotonic and cyclic torsional shearing via 3D digital image correlation

H. Munoz
*Institute of Industrial Science, University of Tokyo, Japan*

M. Umar
*Department of Civil Engineering, University of Tokyo, Japan*

T. Kiyota
*Institute of Industrial Science, University of Tokyo, Japan*

ABSTRACT: A series of monotonic and cyclic tests under simple shear conditions in a torsional shear apparatus were conducted on specimens of saturated medium-dense Toyoura sand. Local strains (i.e. shear strain localisation) together with the global stress-strain response to shearing of the specimens were measured and compared after implementing a non-contact strain-measurement technique via 3-Dimensional Digital image correlation (3D DIC) by an in-house Single-Stereo Camera. The Single-Stereo Camera system was built up based on concepts of reflective optics that allowed the three-dimensional shape and displacement measurements of the deformed specimens. It is found that the rate of shear strain developed inside a localised zone is accelerated as a response change in the specimen from volume expansion to contraction took place. Furthermore, when strain localisation takes place, the global shear strain in the specimen underestimates the shear strain extent experienced in a localised zone, in the order of two-fold.

## 1 INTRODUCTION

The onset of strain localisation is considered an important precursor of strength degradation leading to the failure of soils. During shearing, as shear deformations of a soil element becomes relatively larger, concentration of strain into a narrow zone of intense shearing occurs. Fully understanding of strain localisation onset and its mechanism are essential to study the failure and collapse characteristics of soils in most of earthquake-related geotechnical problems, including liquefaction-induced deformations.

In this instance, previous investigations conducted by Tatsuoka et al. (1986) via drained monotonic torsional shear tests on Toyoura sand under constant vertical and horizontal effective stress, reported that the formation of a shear band in sand specimen was attributed to a sudden reduction of the vertical strain (extension side) accumulated due to the mobilisation of positive dilatancy. Later, Kiyota et al. (2008), after performing undrained torsional shear tests on Toyoura sand, found out that the state response of the deviator stress $q$ (i.e. the difference of vertical to horizontal stress $q = \sigma_v - \sigma_h$,) to be consistent with the generation of the shear band observed by Tatsuoka et al. (1986), i.e. the state at which $q$ suddenly drops. Kiyota et al. (2008) indicate that the shear strain defined at the moment of a sudden drop of $q$ is defined as that the limiting value of shear strain that causes strain localisation.

Kiyota et al (2008)'s limiting shear strain considers global measurement of shear strains in hollow-cylindrical sand specimens (i.e. shear strain in the whole specimen) which is calculated

based on the torsional rotation of the specimen induced by the torsional torque applied to its top end. However, global strain measurement may underestimate the extent of strains in the specimen within the localised zone. This is, due to the effect of sustained shearing, shear strain development within the whole specimen varies significantly due to strain localisation, i.e. strains develops largely, later shown in Figures 4 and 7, within the localised zone in contrast to zones outside the localised zone.

Therefore, in this study digital image correlation (DIC) is used to shed insights into local shear strain development and the formation of shear band(s) under simple shear conditions applied to Toyoura sand under undrained condition by a torsional shear apparatus.

## 2 TORSIONAL SHEARING TESTS

### 2.1 *Torsional loading set-up*

A fully automated torsional apparatus, developed by Kiyota et al. (2008) at the University of Tokyo, shown in Figure 1, was used in this study. The apparatus consist of a belt-driven torsional loading system that is connected to an AC servomotor through electro-magnetic clutches and a series of gears for velocity control. Torque and axial load are measured by a two-component load cell (axial load and torque capacities of 8kN and 0.15kNm, respectively) which is installed inside a pressure cell. Difference in pressure levels between the cell pressure and the pore water pressure are measured by a high-capacity differential pressure transducer (HCDPT) with a capacity of over 600kPa. Volume changes during the consolidation and initial shearing of a specimen are measured by a low-capacity differential pressure transducer (LCDPT). Shear stress amplitude is controlled by a computer, which monitors the outputs from the load cells and calculates the shear stress. The measured shear stress is then corrected to account the effects of membrane force.

### 2.2 *Specimen preparation and shear loading method*

Toyoura sand (Gs = 2.659, $e_{max}$ = 0.951, $e_{min}$ = 0.608), a uniform sand with fines content <0.1%, was used in this investigation. Medium-size hollow cylindrical specimens, with dimensions of 100 mm in outer diameter, 60mm in inner diameter and 200mm in height, were prepared by air pluviation method, thus producing a sand fabric with horizontal bedding planes, at a relative density of 49 ± 3%. High degree of saturation (i.e. Skempton's *B*-value > 0.95) was achieved by the double vacuum method, while circulating de-aired water into the specimens. The specimens were isotropically consolidated by increasing the effective stress state up to a $p_{0'}$ = 100 kPa, with a backpressure of 200 kPa.

Subsequently, to replicate seismic conditions in the field, a constant-amplitude cyclic torsional shear stress ($\tau_{cyclic}$) to a prescribed cyclic stress ratio (CSR) was applied to the sample at a shear strain rate of 0.5%/min. (Table 1). To mimic gentle slope condition, a static shear ratio

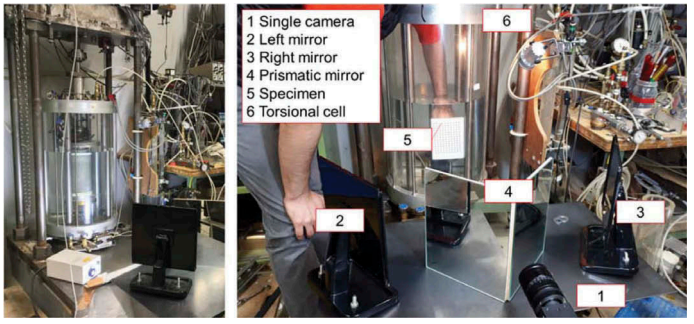


Figure 1. Torsional apparatus and in-house DIC system.

Table 1. Torsional shear tests performed

| Test No. | Relative density $Dr$ (%) | SSR | CSR | Mean effective stress (kPa) $p_0$' | Cyclic damage strain, $\gamma_\Delta$ (%) |
|---|---|---|---|---|---|
| 1 | 47.0 | 0 | Monotonic | 100 | 0 |
| 2 | 47.9 | 0.15 | 0.12 | 100 | 3% |

was applied in drained monotonic shearing (SSR). During the process of undrained cyclic torsional loading, the vertical displacement of the top cap was prevented as much as possible to comply with simple shear conditions similar to that the ground undergoing horizontal seismic excitation.

## 3 SINGLE-CAMERA 3D DIGITAL IMAGE CORRELATION

Digital image correlation (DIC) refers to the class of non-contact measurements methods that acquire images of an object, store images in digital form and perform image analysis to extract the full-field shape, deformation and motion measurements (Sutton M A, 2009).

3D DIC technique encompasses the use of two digital cameras (i.e. Two-Stereo Camera rig systems) positioned in the manner that the surface of the specimen is viewed from two different angles that allows three-dimensional displacement measurements of a deformed object (Munoz et al, 2016a, b, Munoz et al, 2017a, b). Implementing this system generally result costly. Therefore, this study firstly, presents the implementation of a low-cost 3DIC system by using a Single-Stereo Camera, see Yu et al. (2016). Secondly, calibrate the system. The reflective effects of the cell and infilled water on the specimen were taken into account to extract correctly strains in the surface of the specimen. The complete stress-strain behaviour of Toyoura sand in torsional shearing was coupled with the field of shear strains obtained via 3D DIC.

### 3.1 *Speckle pattern preparation*

DIC method relies on a contrasting random texture as speckle pattern in the surface of the specimen (Sutton et al. 2009). To this end, spray painting to speckle pattern the surface of an object is commonly used practice (Munoz et al, 2016a, b, Munoz et al, 2017a, b). In study, a speckle pattern was adhered to the surface of the membrane, which deformed with the surface of the soil sample, so no loss of correlation occurred.

To achieve effective correlation, the speckle pattern was non-repetitive, isotropic and high in contrast, i.e. random pattern exhibiting no bias to an orientation and showing dark blacks and bright whites, adequate in size for high-strain resolution. By doing so, very sensitive defocus was avoided (Sutton et al. 2009).

### 3.2 *Single-camera 3D DIC setup*

Figure 1 shows the Single-Stereo camera system. The camera captured simultaneously the left and right digital grey-scale images. Typical left and right image pairs obtained by the camera during calibration are shown in Figure 2. The camera consisted of two high-resolution monochrome stereo cameras (i.e. Fujinon HF75SA-1, 1:1.8/75mm, 3 Megapixels resolution). Continuous and uniform illumination across the entire specimen was provided by a conveniently adjusted halogen light to ensure adequate contrast. The images were captured by a Snap software using an exposure time of 37 ms.

Prior to the shear torsional tests, each camera was stereo calibrated using a standard target having uniformly spaced markers. To do so, a calibration target was tilted and rotated, in and out of plane, nearby the site occupied by speckled specimen, as shown in Figures 1 and 2.

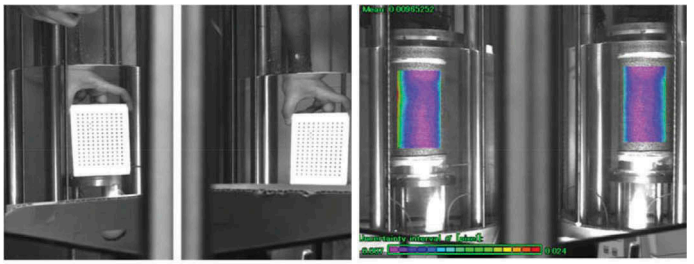

Figure 2. a) Calibration target in water and b) example of results of a good quality pattern and lightening.

The total images acquired during calibration were computed and analysed by VIC-3D software, see Figure 2. VIC-3D software has been used effectively in a number of DIC material testing, e.g. Munoz et al. 2016a,b, 2017a,b. Stereo calibration results produced a standard deviation of residuals of 0.050-0.060 (in pixels), in general for all the tests. During the loading tests, the digital cameras were programmed to capture the images automatically at a frequency 1 Hz. A one-to-one correspondence between load, deformations, and respective digital images during the shear tests allowed studying strain development with stresses. Deformation measurements were concentrated within a portion of the specimen (i.e. the area of interest) as shown in Figure 2. VIC-3D software (produced by Correlated Solutions Inc.) was used for the analysis. This software implements image-processing algorithms for tracking surface coordinates and deformation from image to image. A subset size of 55 pixels was selected for accurate displacements measurements. Upon completion of image processing, the field of strains of the specimen's surface was obtained.

## 4 TEST RESULTS AND DISCUSSION

### 4.1 *Field of shear strain during monotonic shearing*

*Typical global measurements:*
Typical shear stress, deviator stress ($q= \sigma_v-\sigma_h$) and excess pore water pressure versus shear strain (global) of the specimen is shown in Figure 3. Stress-strain curve exhibits the following: a strain hardening behaviour from the beginning of loading at state A towards loading state B and E. Correspondingly, q increased due to the mobilisation of positive dilatancy until state D, consistent with the stress-strain relationship.

However, the amplitude of q suddenly dropped from state D, whereas, shear stress continues to increase further towards state E. The sudden drop of q is regarded as the change of specimen response from volume expansion to contraction by a formation of a shear band. Whereas, shear stress sustainably increased due to mobilization of dilatancy as well as negative buildup pore water pressure locally around and inside the shear band, i.e. from state D to E.

It was deemed that steady state for Toyoura sand under monotonic undrained loading, which is defined as regime at which the specimen continues to deform under constant stress, begins at E at a global shear strain of 12%. The peak strength with this case reached 200 kPa at E.

*Local measurements:*
The corresponding local field of engineering shear strain evaluated by the VIC 3D is shown in Figure 4. The following features were observed:

Strain develops uniformly in the whole specimen in A to B. This can be seen by a single colour pattern, associated to strains in the order of 1%.

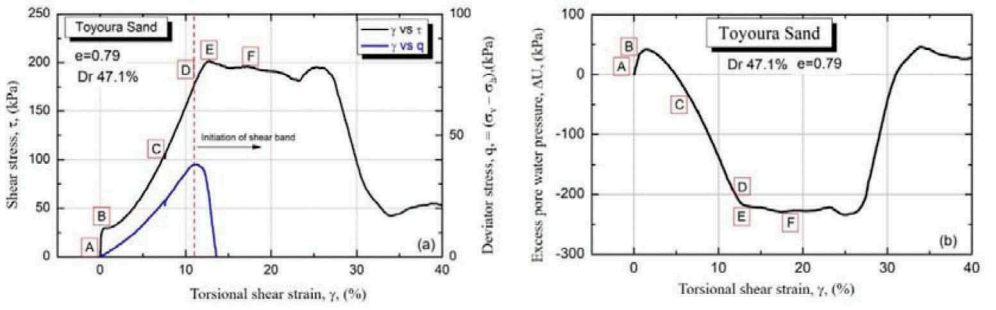


Figure 3. Stress and pore pressure versus strain plots during monotonic torsional shearing. Letters A to F are loading stages.

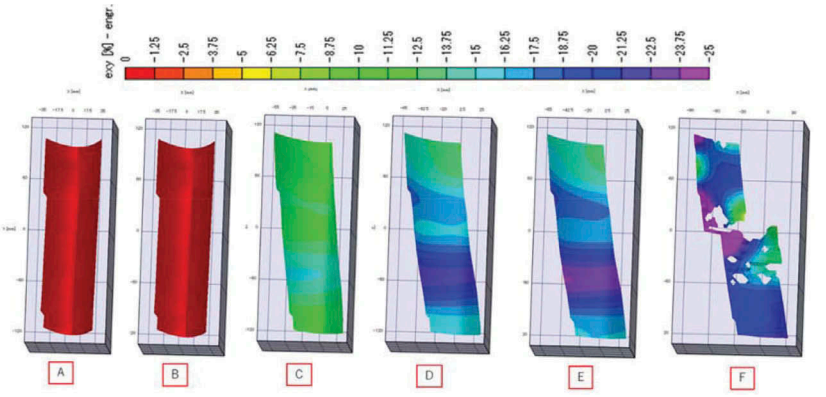


Figure 4. Field of strain in the specimen for loading stages A to F by DIC during monotonic load.

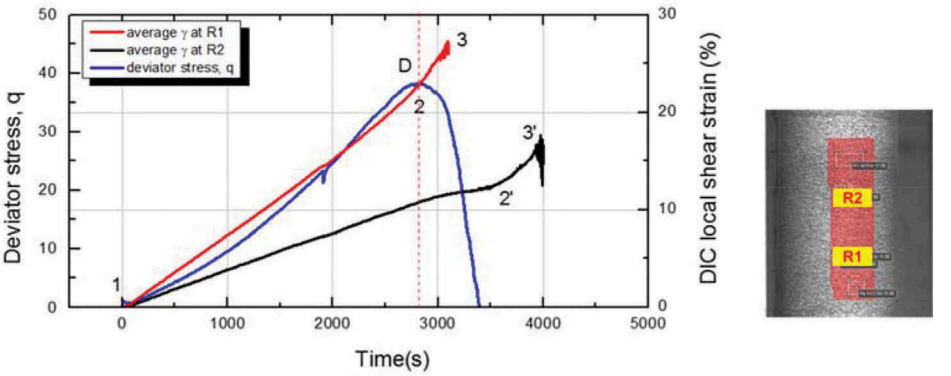


Figure 5. Time history of local shear strain within (R1) and outside (R2) the shear band and q.

Stage C shows strain localising at a thin zone in the sample. In stage C, shear stress is about half of the peak stress at E. At stage C, outside the localised zone (green colour pattern) strains developed in the order of 8%, while inside the localised zones (cyan colour pattern) strains developed in the order of 15% in two localised zones. This feature shows that strains in localised zones can double the strains outside the localised zone.

At stage D, strain develops faster in the localised zones, i.e. in the first localised zone (purple colour pattern) in the order of 23% and the second (blue colour pattern) in the order 17%. Outside the localised zones, strains in the order 12% took place. Again, the ratio of strain in and out the localised zone seems in the two-fold order.

At peak stress at stage E, the shear band zone continues to expand (purple colour pattern) at a strain in order to 27%.

By the above discussion, at stage E, the global shear strain (global strain 12%) seems to underestimate the extent of local shear strains taking place in the localised zone (in the order of 27%) by at least two-fold.

Further examination of the local strain characteristics supports the observations above. In Figure 5, local shear strain within (Region, R1) and outside (Region, R2) the localised zone have been extracted from the DIC measurements and compared with the time history of the change of q during the test. The following observations can be drawn:

Local strain for R1 show a constant rate of strain increment until state D, from point 1 to 2, of about $8x10^{-3}$ %/s. On the other hand, immediately after D takes place and the sample keeps experiencing stress and strains from D towards E, the local rate of strain increment increased faster to about $16x10^{-3}$ %/s, from point 2 to 3. This result indicates that the state of q sudden dropping at D can be associated to a faster increase in the development of strains inside the localised zone, i.e. a two-fold faster.

Similarly, local strain for R2 region show a constant rate of strain increment from 1 to 2′, even after passing over state D and E, about $6x10^{-3}$ %/s, and then an increasing in strain rate from 2′ to 3′ of $14x10^{-3}$ %/s.

In additon the bifurcation between the magnitude of development of strain in R1, from 1 to 2 and 3, together with the magnitude of strain development in R2, from 1 to 2′ and 3′, suggest that the onset of non-homogeneous strains in the whole speciem, associated to the onset of localisation, takes place much before stage D. It seem that the onset of non-homogeneous strains takes place immediately after stage B.

Therefore, the stage where the deviator stress q drops seems to be the state at where shear strains inside the localised zone start to increase at a faster rate. This is important, as a faster increase in shear strains in the shear band can be associated to a faster degradation in strength of the specimen. By this behaviour, it seems that the strength capacity of the specimen after D could only attained and additional extra ~10% to reach the peak strength, from 180 kPa at D to 200 kPa at stage E.

### 4.2 *Field of shear strain during cyclic excitation followed by monotonic loading*

*Typical global measurements*:

Typical shear stress, deviator stress ($q= \sigma_v-\sigma_h$) and excess pore water pressure versus shear strain (global) of the specimen is shown in Figure 6. This case, corresponds to a non-reversal cyclic loading ($\tau_{static} > \tau_{cyclic}$) test. A specific cyclic damage strain ($\gamma_\Delta = 3\%$) from state A to B

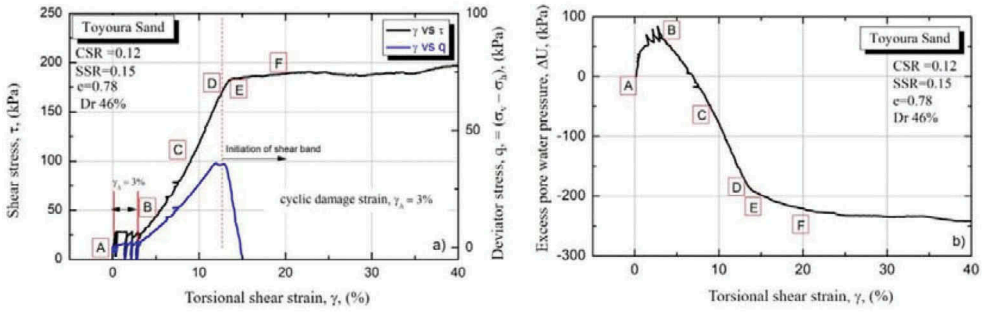


Figure 6. Stress and pore pressure versus strain plots during a cyclic damage torsional shearing. Letters A to F are loading stages.

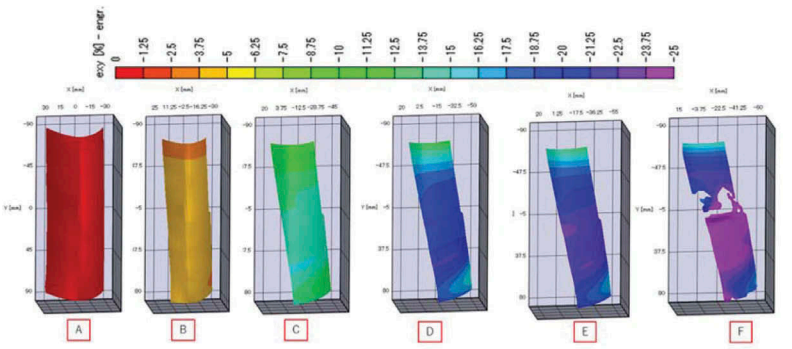


Figure 7. Field of strain in the specimen for loading stages A to F by DIC during cyclic load.

was induced to the specimen (i.e. cyclic excitation), after that a sustained monotonic loading was applied, i.e. from B following C to E until the end of the test, similarly to the monotonic test described above.

At state D in Figure 6, q is suddenly drops, whereas shear stress sustainably increased to the end of the test. The peak strength at E only reached 182 kPa.

*Local measurements*:

Figure 7 shows the field strain developed in the sample evaluated by VIC 3D at different loading states from A to F. This figure suggests the following.

The applied damaging strain of 3% ($\gamma_\Delta$ = 3%) to the specimen induced a nearly homogeneous distribution of strain damage in the whole sample. This feature can be seen by comparing stages A and B in Figure 7, see the homogeneous light orange colour pattern in the sample in stage B.

After the end of the application of the cyclic damaging strain, further application of monotonic shear stress, induced further local shear strain growing in the sample in the order of 10 to 15% distributed nearly homogeneously in the sample as presented stage C. This feature can be seen by a nearly homogeneous green and cyan colour pattern in the sample. Although, a thin zone having a strain about 16% can be observed in stage C.

In Figure 8, local time history of shear strain within (Region, R1) and outside (Region, R2) the localised zone is compared with the drop of q over time. Stage D is located in this figure. Consistent with a monotonic test, the rate in the increase of local strain in region R1 developed showing that before reaching state D, from point 1 to 2, about $7x10^{-3}$ %/s. On the other

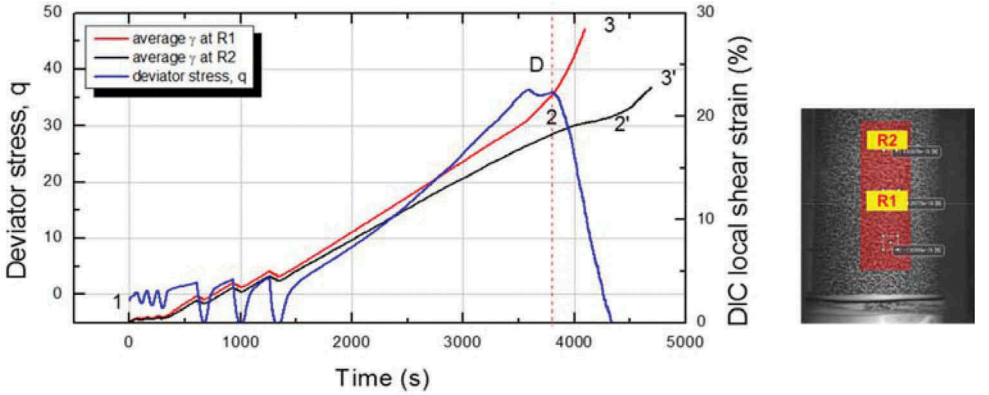


Figure 8. Time history of local shear strain within (R1) and outside (R2) the shear band and q.

hand, immediately after D takes place towards E, the local rate of strain increment increased faster to about $21x10^{-3}$ %/s, from point 2 to 3, a three-fold faster. This result indicates that the state of q sudden dropping at D can be associated to a faster increase in the development of strains inside the localised zone.

This feature can be seen through the colour patter at E, with strain in the order of 20-25% were observed, while at stage F, a broad localised zone was observed in the middle height of the specimen, > 25% (purple colour pattern).

Further comparisons between the rate of strain development to reach D indicates that, with the specimen that was loaded monotonically from beginning to end was slightly faster, i.e. $8x10^{-3}$ %/s, in contrast with the specimen which was initially cyclically damaged to then loaded monotonically, i.e. $7x10^{-3}$ %/s. However, after D takes place, the rate of strain development in the former was $16x10^{-3}$ %/s and much faster about $21x10^{-3}$ %/s in the latter. This is important, as a faster increase in shear strains in the shear band can be associated to a faster degradation in strength of the specimen.

By this behaviour, it seems that the initial damaging strain of 3% induced a faster degradation of the strength capacity of the specimen after D, so that the peak strength with this case only reached 182 kPa, which is much lower than that 200 kPa with the case of the specimen without initial damage, a 10% lower.

Therefore, it can be speculated that an initial damage strain in the specimen take its toll in the specimen by accelerating further the strain development within the localised zone after D which can be the main contributor for a high degradation of strength after D. More research is needed in this regard.

By the above discussion, at stage E the global shear strain seems to underestimate (global strain 14%) the extent of local shear strains taking place in the localised zone (in the order of 27%) by a two-fold.

Studies by Kiyota et al. (2008) and Chiaro et al. (2015a) reported that the strain localisation with initial static shear is independent of the stress or strain loading. However, in this study, it was found localisation and the formation of a shear band may depend on the different rates of strain accumulation, after D, under monotonic and damaging strain cases. This can be a major factor for the degradation of the strength of the specimen. However, more investigation is required on the degradation of undrained strength, as well as the extent of damaging strain to cause strain localisation.

## 5 CONCLUSIONS

An in-house Single-Stereo Camera was employed to evaluate in field shear stain by 3D DIC for non-contact local shear strain measurement. The results shows that local strains taking place in the localise zone (a shear band) was larger, in the order of two-fold, to that the global average shear strain in the whole specimen) calculated based on the torsional force applied to the top of the specimen, in the order of two-fold. It is found that the rate of shear strain development inside a localised zone can be the major contributor to the strength degradation of the specimen.

## ACKNOWLEDGEMENT

The first author would like to thank the Japanese Society for the Promotion of Science (JSPS) for their financial support through the JSPS Fellowship Program to conduct research activities at the University of Tokyo. A trial version of VIC 3D was provided to the second author by Correlated Solutions in Tokyo for the image deformation analysis, which is greatly acknowledged.

## REFERENCES


Chiaro, G., Kiyota, T. & Koseki, J. 2015. Strain localization characteristics of liquefied sands in undrained cyclic torsional shear tests. *Advances in Soil Mechanics and Geotechnical Engineering, IOS Press*, 6 (1): 832-839.

Kiyota, T., Sato, T., Koseki, J. & Mohammad, A. 2008. Behavior of liquefied sands under extremely large strain levels in cyclic torsional shear tests. *Soils and Foundations*, 48(5): 727-739.

Munoz H, Taheri A. & Chanda, E. 2016a. Fracture energy-based brittleness index development and brittleness quantification by pre-peak strength parameters in rock uniaxial compression. *Rock Mechanics and Rock Engineering*, 49 (12): 4587–4606.

Munoz H, Taheri A. & Chanda, E. 2016b. Pre-peak and post-peak rock strain characteristics during uniaxial compression by 3D digital image correlation. *Rock Mechanics and Rock Engineering*, 49 (7): 2541–2554.

Munoz H, Taheri A. & Chanda, E. 2017a. Local damage and progressive localisation in porous sandstone. *Rock Mechanics and Rock Engineering*, 50 (1): 3253–3259.

Munoz H, Taheri A. & Chanda, E. 2017b. Specimen aspect ratio and progressive field strain development of sandstone under uniaxial compression by three-dimensional digital image correlation. Journal of *Rock Mechanics and Geotechnical Engineering*, 9 (1): 599-610.

Tatsuoka, F., Sonoda, S., Hara, K., Fukushima S. & Pradhan, T. B. S. 1986. Failure and deformation of sand in torsional shear. *Soils and Foundations*, 26(4): 79-97.

Yu, L. & Pan B., 2016. Single-camera stereo-digital image correlation with a four-mirror adapter: optimised design and validation. *Optics and Lasers in Engineering*, 87 (1): 120-128.